Building physically-based models for assessing rainfall-induced shallow landslide hazard at the catchment scale: the case study of the Sorrento Peninsula (Italy)

Brunella Balzano, University of Strathclyde, Glasgow,
brunella.balzano@strath.ac.uk

Alessandro Tarantino. University of Strathclyde, Glasgow,
alessandro.tarantino@strath.ac.uk

Marco Valerio Nicotera, Università degli studi di Napoli Federico II, Napoli,
nicotera@unina.it

Giovanni Forte, Università degli studi di Napoli Federico II, Napoli,
giovanni.forte@unina.it

Melania de Falco, Università degli studi di Napoli Federico II, Napoli,
melania.defalco@unina.it

Antonio Santo, Università degli studi di Napoli Federico II, Napoli,
santo@unina.it

Corresponding author:

Professor Alessandro Tarantino

Department of Civil and Environmental Engineering
University of Strathclyde
James Weir Building
75 Montrose Street - Glasgow G1 1XJ, Scotland, UK
E-mail: alessandro.tarantino@strath.ac.uk

Abstract

The assessment of rainfall-induced shallow landslide hazard at the catchment scale poses significant challenge. Traditional empirical approaches for landslide hazard assessment often assume that conditions having caused failure in the past won't change in the future. This assumption may not hold in a climate change scenario. Physically-based models (PBMs) therefore represent the natural approach to include changing climate effects. PBMs would in principle require the combination of a 3-D mechanical and water-flow model. However, a full 3-D finite element model at the catchment scale, with relatively small elements required to capture the pore-water pressure gradients, would have a significant computational cost. For this reason, simplifications to the mechanical (i.e. infinite slope) and water-flow model (i.e. 1-D or hybrid 3-D) are introduced, often based on a-priori assumptions and not corroborated by experimental evidence. The paper presents a methodology to build a PBM in a bottom-up fashion based on geological surveys and geotechnical investigation. The PBM is initially set as simple as possible and then moved to a higher level of complexity if the model is not capable of simulating past landslide events. The approach is presented for the case study of Sorrento Peninsula and two main landslides events recorded during winter 1996-1997.

Key words: **Rainfall, Flow-like landslides, Unsaturated soil, Water flow**

INTRODUCTION

1 Widespread rainfall-induced landslides are one of the major natural hazards and account for
2 significant economic and human losses. The assessment of spatial and temporal landslide
3 hazard at the catchment scale is the key to developing measures to mitigate landslide risk.

4 Landslide hazard can be quantified using empirical approaches. These are based on the
5 correlation of historical records of landslide occurrence with either predisposition or
6 triggering factors, which are leading to susceptibility maps (Andriola et al., 2009; Di
7 Crescenzo et al., 2008; Godt et al., 2008; Wang et al., 2015) and rainfall thresholds (De Vita
8 et al., 2002; Guzzetti et al., 2007) respectively. A major limitation of susceptibility maps is
9 the identification of the factors predisposing the slopes to landsliding, which is based on
10 intuitive understanding of the landslide mechanisms rather than catchment-specific
11 physically-based models. On the other hand, empirical rainfall thresholds are generally based
12 on a minimum or 'safety' threshold for rainfall amounts and/or or intensity-duration that have
13 produced landslides in the past. The conservative nature of the rainfall thresholds may lead to
14 false alarm and the consequent loss of confidence in the early warning system (Intrieri et al.,
15 2012). Overall, traditional empirical models are implicitly based on the assumptions that
16 geomorphological and meteorological conditions having caused failure in the past will
17 remain unchanged in the future. This assumption is not likely to hold in a climate change
18 scenario.

19 These limitations can be overcome if landslide hazard is quantified via physically-based
20 models. These combine a mechanical model for landslides initiation and a hydraulic model
21 for rainwater infiltration. In principle, the analysis at the catchment scale involves 3-D
22 stability analysis and 3-D water flow analysis. While 3-D analysis does not represent a
23 challenge for individual landslides, the computational burden becomes prohibitive if the
24 domain extends over kilometres and the pore-water pressure profile needs to be determined
25 with a resolution of centimetres.

26 As a result, physically based models designed for catchment-scale analysis have been
27 simplified in order to scale down the problem to 2-D or 1-D conditions. Indeed, the majority
28 of the slope failure mechanical models are based the 1-D infinite slope (e.g. Simoni et al.,
29 2008; Godt et al., 2008; Papa et al., 2013, Aristizàbal et al., 2015).

30 On the other hand, various approaches are considered to model rainwater infiltration and
31 lateral flow. A first class of models only consider saturated flow by neglecting the effect of
32 the unsaturated upper part of the soil profile on the water redistribution mechanisms. These
33 include SHALSTAB (Montgomery & Dietrich , 1994) and TRIGRS (Baum et al., 2002) and
34 SHIA_Landslide (Aristizabal et al., 2015). A second group takes into account unsaturated
35 flow. Rigon et al. (2005) consider a hybrid 3-D water flow model by uncoupling lateral from
36 vertical flow. However, the latter is modelled using a relatively coarse discretisation of the
37 flow domain, which may not allow capturing the high pore-water pressure gradients that may
38 develop during a rain-water infiltration process. Savage et al. (2004), Baum et al. (2010), and
39 Papa et al. (2013) consider a 1-D vertical infiltration in order to implement closed-form
40 analytical solutions for the water flow.

41   The common thread between these approaches is that the hydraulic model at the
42   catchment scale is set-up a priori without consideration for the specific hillslope hydrology
43   and landslide mechanisms actually characterising a specific area. The hydraulic model is
44   intended to be 'universal' and therefore adapted to any catchment in a 'top-down' fashion.

45   This paper presents an alternative 'bottom-up' approach to the modelling of physically
46   based models for rainfall-induced shallow landslides. The PBM is built from geological,
47   geomorphological, and geotechnical investigation of historic landslide events. The
48   physically-based model is initially set as simple as possible and then moved to a higher level
49   of complexity if the model is not capable of simulating past landslide events. In other words,
50   a one-dimensional scheme is initially adopted for both mechanical and hydraulic component
51   of the physically-based model. This is then tested against historic landslide events. If the test
52   is negative, the model is scaled-up to a higher level of complexity (e.g. 2-D flow).

53   The approach is illustrated with reference to the case study of the Sorrento Peninsula
54   located in the Campania region in Southern Italy. Two historic landsides representative of the
55   most typical soil profiles have been selected. The landslides are characterised as flow-like
56   landslides (Hungr et al., 2014; Santo et al., 2018). The 'quality' of the physically-based
57   model has been therefore assessed against its capability to reproduce the time of failure and
58   the location of the slip surface identified by the geological survey following the landslide
59   events.

60

STUDY AREA

Geological setting

62 The study area is located on the Tyrrhenian coast of Campania. During the Plio-Quaternary
63 times, important regional faults associated with the extension of the Tyrrhenian area
64 generated a major tectonic depression named the Campania graben (Southern Italy). The
65 structural horsts bounding this graben include the carbonate Sorrento Peninsula–Lattari
66 Mountains, the Partenio Mountains, the Caserta Hills, Pizzo D'Alvano mountain, and
67 Maggiore Mountain. These mountains consist of more than 1500-m-thick Mesozoic
68 dolomites and limestones.

69 The most recent deposits on the limestone formation are quaternary continental debris and
70 pyroclastic deposits; the latter are a few metres thick and associated with the Late
71 Pleistocene–Holocene Plinian eruptions of the Campi Flegrei and Somma-Vesuvio volcanic
72 areas. The fallout products of these volcanic areas were deposited mostly on the carbonate
73 formation. Studies of the dispersion axis of pyroclastic deposits have shown that the most
74 superficial layers (pumices and pyroclastic cover) in the area of the Sorrento Peninsula are
75 associated with the AD 79 eruption.

76 The geomorphological pattern is characterized by high relief slopes, with peaks often
77 reaching altitudes greater than 1000 m. In most cases, these slopes have been associated with
78 fault scarps generated by various phases of block faulting that occurred during the late
79 Pliocene and the lower and middle Pleistocene. Slope replacement then took place, producing
80 linear slopes characterized by a rectilinear cross profile with a medium slope angle of about
81 35° (Brancaccio et al., 1999). This morphological context affected the deposition of the
82 Holocene pyroclastic fall deposits. The presence of pyroclastic covers, especially in the
83 steeper areas, makes wide sectors of these slopes particularly susceptible to the triggering of
84 debris slides–rapid earth flows. These are usually triggered by short duration intense
85 meteorological events, particularly after prolonged periods of antecedent rainfall. Due to their
86 high degree of fluidity they can travel over long distances, thereby increasing their power of
87 destruction. Many landslides events took place in the past, very often with tragic
88 consequences on goods and human lives.

The landslide events of January 1997

90 An intense period of precipitation occurred in Campania from January 9th to 11th, 1997.
91 Rainfall was particularly intense in the western areas of the region, namely, the Sorrento
92 Peninsula and the Lattari Mountains. A 3-day cumulative rainfall of about 280 mm was
93 registered at those locations, preceded by a 4-month period of high cumulative rainfall. On
94 the same days, several hundreds of landslides were triggered in the Campania region. Most of
95 these landslides (about 400) occurred in the Sorrento Peninsula–Lattari Mountains.
96 Landslides involving natural slopes were mainly superficial, sometimes turning into
97 debris/earth flows. Small-scale falls and slides occurred on cut slopes (Di Crescenzo and
98 Santo, 1999).
99 This work deals with two events occurred on the10th of January 1997: the Gragnano and
100 Corbara's landslides (Figure 1).

Gragnano

102 The Gragnano (1997) landslide was triggered on the northern slope of Pendolo Mt., an area
103 severely affected by those events in the past. The area is characterized by a high grade of
104 susceptibility, mainly due to high values of slope angles (around 35°) and a fair continuity of
105 the pyroclastic material between 0.5 -2.5 m thick. The carbonate bedrock in the area is
106 strongly fractured and karstified and it is covered by an ash-fall layer characterized by a high
107 clay content (C1 and C2). The latter is covered by the products of 79 AD Plinian eruption, i.e.
108 coarse pumices (B), ashes (A2) and soil (A1) as shown in Figure 2

109 This landslide event occurred around 1:30pm of the 10th of January 1997 and took place in an
110 area affected by another previous event, activated at 9 am of the very same day (Figure 3a). It
111 seems that before the major landslide events, the soil itself showed some premonitory cuts on
112 its surface. The average length of the landslide is roughly 220 m, involving 4500 m^3 of
113 material (Figure 3b).

114

Corbara

116 This event took place adjacent to the road that leads to the Chiunzi Pass and was
117 characterised by a total length of 250m. It started as a translational shallow landslide that
118 evolved into a debris flow. In this case, it was not possible to identify the soil profile at the
119 landslide scarp due to remedial works that took place immediately after the event. The soil
120 profile was characterised by boreholes and/or trenches out by the Geology Department of
121 University of Naples Federico II just close to the landslide site and is shown in Figure 4. In
122 this case, the bedrock appears to be covered by a very thin layer (0.3-0.4 m) of ashes,
123 overlain by a 0.8-0.9 m layer of yellow pumices and a 0.9m layer of pedogenised pyroclastic
124 soil.

MATERIALS

125 Three major soil types cover the limestone bedrock (Figure 5):

126 • A top layer of pyroclastic soil, which has been affected by biogeochemical processes as a
127   result of the direct and indirect action of microorganism and vegetation (A1). This layer
128   originally formed during the last stage of the 79 AD eruption.
129 • Pumices (P). This layer was deposited during the early stage of the 79 AD eruption.
130 • Ashes, deriving from an ancient eruption (130000 years ago ca.) from Campi Flegrei
131   volcanic areas (C1 and C2)

132 The hydro-mechanical characterisation of these soils was carried using different
133 approaches depending on the layer in question. The choice hydro-mechanical properties of
134 the layers A1, P, and C1 was based on the characteristics of similar soils at a site located in
135 another area of the Campania region due to the similarity in terms of the grain-size
136 distribution and volcanic origin (Monteforte Irpino, Figure 4). The hydraulic properties of
137 the soils at the Monteforte Irpino site were indeed investigated extensively via laboratory
138 testing and field monitoring (Pirone et al., 2015; Pirone et al. 2016). A typical soil profile at
139 the Monteforte Irpino site is reported in Figure 6.

140   The hydraulic characterisation of soil C2 was carried out via laboratory testing of single
141 sample taken from the C2 layer in the Sorrento Peninsula. This soil type is not present in the
142 Monteforte Irpino soil profile and, hence, its properties could not be borrowed from any of
143 the soils at this site.

Hydraulic Properties

Soil A1 and C1

146 Figure 7 shows the comparison between the grain size distributions of Soil 1 from Monteforte
147 Irpino and Soil A1 from the Sorrento Peninsula (a) and between Soil 6 from Monteforte
148 Irpino and Soil C1 from the Sorrento Peninsula (b). Due to the similarity of the GSD, it was
149 assumed that hydraulic and mechanical properties are also similar.

150   Figure 8a shows the water retention data derived from field measurements in Soil 1. The
151 water retention curve has been represented with suction in linear scale. It represents the water
152 retention behaviour up to saturation in the negative range of suction (positive range of pore-
153 water pressure). The main drying and main wetting curves derived from laboratory
154 measurements are also shown in the figure (Pirone et al., 2015). The field data lie between
155 the main drying and main wetting curves, i.e. they appear to populate scanning paths. Since
156 the field data tends to cover a relatively narrow region, water retention behaviour of Soil 1
157 was modelled via a single (scanning) curve. A modified Van Genuchten function (Van
158 Genuchten 1980) has been used to model the water retention behaviour for Soil 1.

$$\theta = \theta_r + (\theta_s - \theta_r)(1 + \alpha(u_w^* + s)^{\,n})^{-(1-\frac{1}{n})}$$

[1]

159 here

- θ_s is the volumetric water content at saturation
- θ_r is the residual volumetric water content
- u_w^* is the value of (positive) pore water pressure at which the degree of saturation becomes equal to 1 ($\theta = \theta_s$)
- α and n are fitting parameters

165   Figure 8b shows the field measurements of hydraulic conductivity for the Soil 1 (Pirone
166 et al. 2015). For comparison, the hydraulic conductivity derived in the laboratory from
167 undisturbed samples is also shown in the figure. The saturated hydraulic conductivity
168 measured in the field appears to be higher than the one measured in the laboratory by one
169 order of magnitude. This can be attributed to macro-porosities that are present in the field
170 due to the effect of microbial activity and presence of roots in the rhizosphere. A modified
171 Mualem-Van Genuchten function (Mualem, 1976) has been used to model the hydraulic
172 conductivity behaviour for Soil 1.

$$k = k_s S_r^l [1 - \left(1 - S_r^{n/n-1}\right)^{1-\frac{1}{n}}]^2$$

[2]

173 where

- k_s is the saturated hydraulic conductivity,

175	•	S_r is the degree of saturation
176	•	l is a fitting parameter
177	•	n is the fitting parameter already introduced for Equation 1

Figure 9a shows the water retention data derived from field measurements in Soil 6. The main drying curve derived from laboratory measurements is also shown in the figure (Pirone, et al., 2015). By comparison with Figure 9a, it can be inferred that field data for Soil 6 also populate scanning paths. Equation 1 was also used to model the (scanning) water retention curve for Soil 6.

Figure 9b shows the unsaturated hydraulic conductivity function for Soil 6 as derived from laboratory testing on undisturbed samples (Pirone et al., 2016) and also the laboratory measurements of saturated hydraulic conductivity on a second series undisturbed samples. As field data for hydraulic conductivity of Soil 6 are not available, an assumption had to be made regarding the field scaling factor for the hydraulic conductivity (i.e. the ratio between the values of hydraulic conductivity in the field and the laboratory respectively).

It can be reasonably inferred that smaller number and size of macro-pores are present in C1 as compared to A1 due to reduced microbial activity and presence of roots. A scaling factor of 5 has therefore been used for Soil C1 as compared to the scaling factor of 10 observed for Soil A1. The parameters used to model the soil A1 and C1 are reported in Table 1.

Pumices

The pumices layer present in the two sites of the Sorrento Peninsula originated during the eruption of Vesuvius in 79AD; these pumices appear to have a grain size distribution similar to that of soil layer 5 at the Monteforte Irpino site as shown by the comparison between the grain size distributions in Figure 10. However, soil layer 5 has been identified as a fall deposit produced by a more ancient eruption of Vesuvius (i.e. Avellino eruption 3760 b.p.). Evangelista et al. (2005) tested in the laboratory on reconstituted samples, along a main drying path, the water retention behaviour of Avellino pumices; in particular two tests were carried out, by considering the pumice particles initially dry or water-soaked.

Water retention appears to be bi-modal and was therefore modelled by considering the superposition of two Van Genuchten-type functions:

$$\vartheta = \vartheta_{res,l} + \frac{\left(\vartheta_{sat,l} - \vartheta_{res,l}\right)}{\left(1 + \left(\alpha_l \cdot s\right)^{n_l}\right)^{m_l}} + \vartheta_{res,h} + \frac{\left(\vartheta_{sat,h} - \vartheta_{res,h}\right)}{\left(1 + \left(\alpha_h \cdot s\right)^{n_h}\right)^{m_h}} \qquad [3]$$

Two sets of parameters should be assigned for the functions in the high and low range of suction respectively. In particular, α_l, n_l, m_l and $\theta_{sat,l}$, $\theta_{res,l}$ are the fitting parameters for the low range of suction and α_h, n_h, m_h and $\theta_{sat,h}$, $\theta_{res,h}$ are the fitting parameters for the high range of suction. The following constraints have to be imposed to liaise the parameters of the two functions with the overall volumetric water contents at saturation and at the residual state:

$$\vartheta_{sat,low} = \vartheta_{sat} - \vartheta_{res,low} \tag{4}$$

$$\vartheta_{sat,high} = \vartheta_{res,low} \tag{5}$$

$$\vartheta_{res,high} = \vartheta_{res} - \vartheta_{res,low} \tag{6}$$

211 The best-fitting parameters for the low and high suction range are reported in Table 3 and
212 Table 4 respectively.

213 The saturated hydraulic conductivity of the Avellino pumice was available from
214 laboratory measurements and found to be equal to 0.1 m/s.

215 Unfortunately, no experimental tests have been carried out to investigate the hydraulic
216 conductivity in the unsaturated range. A very classical model was then considered for the
217 hydraulic conductivity derived by combining the Mualem's model (Mualem, 1974) and the
218 Brooks & Corey's model (Brooks & Corey's, 1964)

$$K[m/sec] = K_{sat} \cdot \left(\frac{\vartheta}{n^*}\right)^{\frac{(2+2.5\lambda)}{\lambda}} \tag{7}$$

219 where θ is the volumetric water content, n* is the porosity, and λ is the sope of the water
220 retention curve in a log-log plot. The parameter λ was tentatively derived by linearizing the
221 bi-modal water retention curve as shown in Figure 11(λ=0.273).

222 **Soil C2**

223 The soil C2 could not be compared to any soil present at the Monteforte Irpino experimental
224 site. For this layer, a single water retention test was performed on a single undisturbed sample
225 taken from a site close to the landslides events. The water retention and hydraulic
226 conductivity function were determined by inverse analysis of an evaporation process
227 according to the approach presented by Nicotera et al. (2010). The curve determined
228 experimentally was associated with a main drying path. According to Figure 12, a scanning
229 path is likely to represent the water retention behaviour in the field more realistically than a
230 main drying path. As a first approximation, the scanning path was derived by shifting the
231 main drying water retention curve in order to have a degree of saturation at zero suction equal
232 to 80% (rather than 100%) as shown in Figure 12a, similarly to what has been observed in
233 soil A1 at the Monteforte Irpino site (Figure 6).

234 The hydraulic conductivity function was derived experimentally as a function of the
235 degree of saturation according to Equation 1. The hydraulic conductivity function is shown in
236 Figure 12b as a function of suction based on the 'scanning' water retention curve shown in
237 Figure 12a.

238

239 **Mechanical Properties**

240 The shear strength properties for the soils A1, P, and C1, were again borrowed from the soils
241 present at the Monteforte Irpino experimental site (associated with soils 1, 3, and 4
242 respectively in Figure 6). Critical state values of friction angle reported in Table 5 have been
243 characterised by Papa (2008) and discussed by Sorbino and Nicotera (2013). For the soil C2,
244 none of the soils present at the Monteforte Irpino experimental site have 'identical' grain-size
245 distribution (as occurring for soils A1, P, and C1). The soil at Monteforte Irpino experimental
246 site closest to C2 in terms of grain-size distribution and plasticity index is the Soil 8 in Figure
247 6. The friction angle was therefore borrowed from this Soil 8 according to Papa (2008).

248 Finally, it was assumed that the saturated failure envelope is characterised by zero
249 effective cohesion with the only exception of Soil A1 where a cohesion of 5 kPa was
250 tentatively assigned to simulate root mechanical reinforcing.

251 The shear strength in the unsaturated range was formulated as follows according to
252 Nicotera et al. (2015) as follows:

$$\tau = (\sigma + s \cdot S_r) \cdot tan\phi'$$

[8]

253 where σ is the normal total stress s is the suction, S_r is the degree of saturation, and ϕ' is the
254 critical state friction angle.

HYDRO-MECHANICAL MODEL

255 The two landslide events have been modelled numerically in order to reproduce the failure
256 occurred on the 10th of January 1997 following heavy rainfall. Rain-water infiltration has
257 been modelled assuming a rigid soil-skeleton (i.e. without considering any coupling with
258 mechanical deformation). The onset of failure was modelled by assuming the soils to have a
259 rigid-perfectly plastic behaviour

260 **Hydraulic model**

261 Rainwater infiltration within the slope was modelled using Darcy's law, extended to the case
262 of unsaturated soils:

$$\vec{v} = -\mathbf{K}\, grad(\Psi) = -\mathbf{K} grad\left(z + \frac{u_w}{\gamma_w}\right)$$

[9]

263 where $\vec{v}$ = flow velocity vector; ψ = piezometric head; $\mathbf{K}$ = hydraulic conductivity; u_w = pore
264 water pressure; γ_w = density of soil water; and z = vertical coordinate increasing upward. The
265 hydraulic conductivity depends is a function of the pore water pressure.

266   The mass balance equation for liquid water can be written as follows:

$$div\,\vec{v} + \frac{\partial \theta}{\partial t} = 0$$

[10]

267 where θ = volumetric water content (ratio of water volume to total volume); and t = time. By
268 substituting Equation 9 in Equation 10, the Richard's equation in terms of piezometric head is
269 obtained:

$$C\frac{\partial \Psi}{\partial t} = div[\mathbf{K} grad(\Psi)]$$

[11]

270 where $C = \gamma_w(\partial\theta/\partial u_w)$, referred to as water capacity of the soil.

271   The volumetric water content θ appearing in Equation 10 is given by:

$$\theta = n^* S_r$$

[12]

272 where n^* = porosity; and S_r = degree of saturation. In general, n^* depends on pore water
273 pressure and, as a result, infiltration is coupled with the mechanical response of the soil.
274 However, shallow landslides often occur in coarse-grained soils that have been subject to
275 countless cycles of drying and wetting. Hence, it then appears reasonable to assume the soil
276 skeleton to be incompressible with respect to pore water pressure changes. As a result, the
277 problem of unsaturated flow can be uncoupled and Equation 11 can be used for calculating
278 the change of pore water pressure with depth and time. The water flow Equation 11 was
279 solved numerically via the FEM using the module SEEP/W of the software Geostudio.

Geometry

281 Rain-water infiltration has been modelled by tentatively assuming infinite slope 'one-
282 dimensional' water flow. This assumption has then been tested as explained later in the paper.
283 It will be shown that the 1-D model is appropriate for the slopes in question. However, if the
284 test had been negative, a 2-D numerical model would have been considered in a second
285 iteration. The soil profiles have been modelled accordingly to the stratigraphy reported in
286 Figure 13.

287 **Boundary Conditions**

288 The boundary conditions for the numerical model are schematized in Figure 14 and consist
289 of:

290 • Water inflow imposed at the top boundary (to simulate rainfall)
291 • Water outflow at 10 cm below the ground surface (to simulate evapotranspiration
292   from the root system)
293 • Impermeable bottom boundary (to simulate the bedrock)

294 *Rainfall data*

295 Rainfall data were taken from rain gauges as close as possible to the landslide areas. Figure
296 15a-b show the rainfall registered from the 1st of January 1994 until the 31st of January 1997
297 for Gragnano and Corbara respectively.

298 *Potential evapo-transpiration*

299 The evapo-transpiration fluxes in the energy-limited regime (potential evapo-transpiration)
300 were calculated using the Penmann-Monteith equation (Monteith, 1965)

$$ET_0 = \frac{\Delta(1-\alpha)R + \rho_a c_p e_s \frac{(1-RH)}{r_a}}{\Delta + \gamma(1+\frac{r_s}{r_a})}$$ [13]

301 where

302 • Δ is the slope of the saturated vapour pressure curve ($\delta e_o/\ \delta T$, where e_o = saturated vapour
303   pressure (kPa) and T_{mean} = daily mean temperature (°C))
304 • R is the (short wave) radiation flux
305 • α is the albedo assumed to be equal to 0.23 according to Allen et al. (1998)
306 • γ is the psychrometric constant (kPa ° C^{-1}) given by 0.665 10^{-3} P where P is the
307   atmospheric pressure (kPa)
308 • ρ_a is the air density
309 • c_p is the specific heat of dry air, assumed 1.013 10^{-3} (MJ kg^{-1} °C^{-1}),
310 • e_s is the mean saturated vapour pressure
311 • r_a is the bulk surface aerodynamic resistance for water vapour
312 • RH is the ambient relative humidity
313 • r_s is the canopy surface resistance

314 The aerodynamic resistance r_a was in turn modelled according to Allen et al. (1998)

$$r_a = \frac{ln\left[\frac{z_m - d}{z_{om}}\right] ln\left[\frac{z_h - d}{z_{oh}}\right]}{k^2 u_z}$$

[14]

where

- z_m height of wind measurements (m),
- z_h height of humidity measurements (m),
- d zero plane displacement height (m),
- z_{om} roughness length governing momentum transfer (m),
- z_{oh} roughness length governing transfer of heat and vapour (m),
- k von Karman's constant, 0.41 (-),
- u_z wind speed at height z (m s^{-1}).

and the canopy resistance r_c was assumed equal to 50 s m^{-1} according to the value suggested by Abtew et al. (1995) for the family of chestnuts.

The radiation R, the relative humidity RH, the temperature T, and wind speed u were taken from an open access database (www.ilmeteo.it for temperature, relative humidity, and wind speed and www.solaritaly.enea.it for solar radiation). The albedo α was assumed equal to 0.15 according to Oke (1992). The monthly evapo-transpiration fluxes calculated using Eq. [9] are shown in Figure 16 for both the sites of Gragnano and Corbara.

Water-limited evapo-transpiration

Potential evapotranspiration only occurs if the soil-plant system can deliver the water flow demanded by the atmosphere. For the case of high potential evapotranspiration rate and/or low soil moisture content, this condition cannot be met and the actual water outflow is dictated by soil-plant system rather than the meteorological conditions (water-limited regime).

The reduction of water outflow in the water limited regime can be modelled via a reduction function that relates the ratio between actual and potential evapotranspiration to the suction at the water extraction. Figure 17 shows a typical reduction function as suggested by Feddes, et al.(1978). As shown, as long as the suction values stay lower than s0, the system is able to accommodate the atmospheric demand (actual evaporation = potential evaporation). When the suction reaches the value s0, the system's water storage is not sufficient to accommodate the potential evapotranspiration any more. Therefore, for $s>s_0$, the actual evaporative flux decreases until the system is completely dry ($s=s_1$).

An approach was developed in this work to calibrate the parameters of the reduction function, the suction value s_0 and the slope of the reduction function δ. A soil column 1.6 m high characterised by the same soil profile at the Gragnano landslide site (Figure 13a) was considered. The column was subjected to the boundary condition derived from Eq. 13 for the period starting 01/01/1995.

Two different initial hydrostatic conditions, associated with suction at the base of the column equal to 0 and 10 kPa respectively, were considered. Figure 18a shows the evolution of suction at the top of the column over time. It can be seen that suction tends to increase very

352 rapidly after a period of time, which depends on the initial condition. The very rapid increase
353 of suction is associated with the attainment of the water-limited regime; the soil column is no
354 longer able to deliver the 8mm/day imposed at the boundary.

355 Figure 18b shows the time derivative of suction with respect to suction. It can be
356 observed that i) time derivative is now independent of the initial condition and ii) the suction
357 marking the transition to the water limited regime can be clearly identified. The suction of
358 1000 kPa has been chosen for s_0.

359 To characterise the water limited regime, the assumption has been made that suction at
360 the extraction point remains constant in the water limited regime. This assumption is built
361 upon the observation that suction in the leaves tends to remain constant in the water-limited
362 regime (Duursma et al., 2008). The parameter δ was then selected by trial and error in order
363 to reproduce a constant value of suction in the water limited regime as shown in Figure 19.
364 The reduction function calibrated on the Gragnano soil profile is shown in Figure 20.

Initial Condition for the transient analysis

366 The landslide events occurred on the 10 January 1997. The numerical analysis of water flow
367 was then carried out between 1 January 1996 and 28 February 1997. The numerical analysis
368 requires an assumption about the initial condition in terms of pore-water pressure profile at
369 the start of the analysis (1 January 1996). This initial condition is unknown and cannot be
370 assumed a priori due to its significant influence on the numerical results, i.e. the slope may or
371 may not experience failure in the numerical simulation depending on the (arbitrary) choice of
372 the initial hydraulic condition.

373 An approach was then developed in this work to derive the initial hydraulic condition. Since
374 the same approach is also used to test and validate the hydraulic model, it is discussed
375 separately in the following section.

Validation of the hydraulic model

377 A distinct numerical analysis was carried out by considering rainfall and evapotranspiration
378 occurring in 1994 and 1995 and repeating the same rainfall and evapotranspiration pattern for
379 three times for Gragnano (for a total of 6 years) and for 1 time for Corbara (for a total of 2
380 years). Three steady-state 'infinite slope' initial conditions were selected, assuming that
381 suction at the bottom of the soil profile was equal to 10 kPa, 40 kPa and 100 kPa respectively.

382 The results from this analysis are shown in Figure 21 in terms of suction at the bottom
383 boundary versus time. It can be observed that:

    i)   The effect of the (arbitrary) initial condition is eventually cancelled if the water
385 flow analysis is carried out for a time sufficiently long (after about 4 years for
386 Gragnano and 0.2 years for Corbara).

    ii)   Once the suctions generated by the three different initial conditions converge,
388 suction tends to fluctuate around an average value that tends to remain constant
389 over time.

390 Condition i) allows selecting the initial condition in an unambiguous way. Once
391 convergence has occurred, the time evolution of suction over 1995 can be assumed to be the
392 actual one. As a result, the suction profile at 31/12/1995 can be assumed as the initial
393 condition for the analysis to be carried out for the period 01/01/1996 to 28/02/1997.

394   The condition ii) can be taken as an evidence of the robustness of the hydraulic model
395 assumed in terms of boundary conditions. In fact, one would expect that a hydrological
396 balance is accomplished over a relatively long period. If the hydraulic model (including its
397 boundary conditions) is not set properly, it may occur that the slope becomes either
398 oversaturated or entirely dry over time. In this case, it appears that the 1-D 'infinite slope'
399 hydraulic model is appropriate for the slopes of Corbara and Gragnano. Should the test on
400 hydrological balance have failed, a different model should have been selected (e.g. 2-D) and
401 the iteration started again.

402 **Mechanical model**

403   **Geometry**

404 The length L and depth D of the landslides at the release zone measured during the
405 geomorphological survey after the landslide event are reported in Table 7. It can be observed
406 that the ratio D/L is less than 1/10 and the onset of failure was therefore modelled by
407 assuming an 'infinite slope' failure mechanism.

408   **Factor of safety**

409 The factor of safety at any depth can be derived via the limit equilibrium method. By
410 considering the shear strength criterion given by Equation 15, the following equation can be
411 derived

$$\text{FoS} = \frac{\tan\phi'}{\tan\beta} + \frac{-u_w S_r \cdot \tan\phi'}{(\bar{\gamma}H) \cdot \sin\beta \cdot \cos\beta} \qquad [15]$$

412 where H is the depth of the failure surface, β is the inclination of the slope, and $\bar{\gamma}$ is the
413 average unit weight given by:

$$\bar{\gamma} = \frac{1}{H} \int_0^H [\gamma_s(1 - n^*) + \gamma_w n^* S_r]dz \qquad [16]$$

414 where γ_s and γ_w are the unit weight of solids and water respectively, and n* is the porosity.

RESULTS

415 To derive the factor of safety versus time, the water flow equation (Eq. 11) was first solved
416 numerically considering the hydraulic properties, initial condition, and boundary conditions
417 discussed in the previous section. In particular, the water retention and hydraulic conductivity
418 functions shown in Figure 8, Figure 9, Figure 11 and Figure 12 were considered for the
419 materials forming the slope as shown in Figure 13. The boundary conditions shown in Figure
420 14 and discussed in the "Hydro-mechanical Model" Section were considered.

421   Figure 22 shows the evolution of the Factor of Safety (FoS) for the case studies analysed
422 from 1 January 1996 until the day where a FoS equal to unity was attained at one depth at
423 least. To highlight the evolution of the FoS, Figure 23 shows the evolution of the minimum
424 FoS from January 1996 to the 10th of January 1997 when the landslide events occurred

425   The numerical simulation returned failure conditions on the 12 January 1997 for the case
426   of Corbara (progressive day no. 377) and 11 January 1997 (progressive day no. 376) for the
427   case of Gragnano. These times compare favourably well with the date of 10 January 2017
428   where landslides occurred. It is also worth observing that the numerical simulation returns a
429   failure surface developing at the interface between C1 and C2 for Gragnano and at the
430   interface between C1 and the bedrock for Corbara. Again, this is consistent with the field
431   observation following the survey after the landslide event. Overall, these results returned by
432   the numerical simulation corroborate the approach adopted to formulate the physically-based
433   hydro-mechanical model for the two landslides.

434   To have a better insight into the hydrological mechanisms triggering the landslides in the
435   Sorrento Peninsula, it is worth exploring the pore-water profiles at the time of failure as
436   shown in Figure 24. A sharp change in hydraulic conductivity occurs at the interface between
437   the ashes (C1) and the compacted ashes (C2) for the case of Gragnano (a) and at the interface
438   between the ashes (C1) and the bedrock for the case of Corbara (b). This causes the formation
439   of a perched water table as inferred from the positive pressure generated above the C1-C2
440   interface for Gragnano and C1-Bedrock for Corbara. Positive pore-water pressures then cause
441   a drop in normal effective stress and, hence, shear strength until failure is eventually
442   triggered.

443

CONCLUSIONS

444   This paper has presented an approach to formulate physically-based models for shallow
445   landslides. The model was built in a 'bottom-up' fashion based on geological,
446   geomorphological, and geotechnical investigation of historic landslides.

447   These investigations allowed designing typical soil profiles and characterising
448   mechanically and hydraulically the materials forming the different geological layers present
449   in the area. The hydraulic model was then tentatively set as one-dimensional and tested
450   against i) its ability to reproduce a satisfactory hydrologic balance over a relatively long
451   period with the slope subjected to real rainfall and evapotranspiration pattern and ii) its
452   capability of losing memory of the initial condition inevitably set up in an arbitrary fashion.
453   The hydrological balance was considered as a 'hypothesis test' for the hydraulic model. If the
454   test is positive, which was the case for the shallow slopes considered in this study, there will
455   be no need to develop more sophisticated (and computationally expensive) hydraulic models
456   in two or three dimensions. This clearly simplifies the numerical modelling of the landslide
457   initiation at the catchment scale. At the same time, the use of a hydraulic 1-D model could be
458   corroborated by numerical evidence and was not cast a-priori as often the case in numerical
459   studies of shallow landslide initiation at the catchment scale reported in the literature.

460   The hydraulic model (including its boundary and initial conditions) was then coupled
461   with a simple mechanical model and tested against its capability of reproducing the time of
462   failure and the location of the slip surface identified by the geological survey following the
463   landslide events. Again, this was taken as 'hypothesis test' for the hydro-mechanical
464   physically-based model for the Sorrento Peninsula catchment.

465   The model has shown to adequately capture time and location of failure for the two
466   historical landslide events considered. This makes it possible to generalise the physically-
467   based model to the entire catchment with fair confidence and use is as a basis to develop
468   hazard maps and/or hydrological triggering thresholds used in early-warning systems.

469

470

REFERENCES

Abtew, W., Newman, S., Pietro, K. & Kosier , T., 1995. Canopy Resistance Studies of Cattalis. American Society of Agricultural and Biological Engineers, 38(1), pp. 113-119.

Allen, R. G., Pereira, L. S., Raes, D. & Smith, M., 1998. Crop evapotranspiration: Guidelines for computing crop waterrequirements. FAO Irrigation and Drainage Paper 56, s.l.: s.n.

Andriola P., Chirico G.B., de Falco M., Di Crescenzo G., Santo A. (2009). A comparison between physically-based models and a semiquantitative methodology for assessing susceptibility to flowslides triggering in pyroclastic deposits of southern Italy. Geografia Fisica e Dinamica Quaternaria, 32, 2, pp. 213 - 226.

Aristizabal , E., Velez , J., Martinez , H. & Jaboyedoff , M., 2015. SHIA_Landslide: a distributed conceptual and physically based model to forecast the temporal and spatial occurrence of shallow landslides triggered by rainfall in tropical and mountainous basins.. Landslides, 13(3), pp. 497-517.

Baum, . R. . L., Godt, . J. W. & Savage ,W. Z., 2010. Estimating the timing and location of shallow rainfall-induced landslides using a model for transient, unsaturated infiltration. J. Geophys. Res.- Earth, Volume 115.

Baum, R. L., Savage, W. Z. & Godt, J. W., 2002. TRIGRS—A Fortran program for transient rainfall infiltration and gridbased regional slope-stability analysis, Reston, Virginia: U.S. Geological Survey.

De Vita, P. & Piscopo, V., 2002. Influences of hydrological and hydrogeological conditions on debris. Natural Hazards and Earth System Sciences, pp. 27-35.

Di Crescenzo, G. et al., 2008. Proposal of a new semiquantitative methodology for flowsides triggering susceptibility assessment in the carbonate slope contexts of Campania(Southern Italy). Italian Journal of Engineering Geology and Environment, pp. 61-79.

Di Crescenzo, G. & Santo, A., 1999. Analisi geomorfologica delle frane da scorrimento-colata rapida in depositi piroclastici della penisola sorrentina (Campania). Geografia Fisica e Dinamica Quaternaria, Volume 22, pp. 57-72.

Di Crescenzo, G. & Santo, A., 2005. Debris slides-rapid earth flows in the carbonate massifs of the Campania region (Southern Italy): morphological and morphometric data for evaluating triggering susceptibility. Geomorphology, 66(1-4), pp. 255-276.

Evangelista, A., Nicotera, M. V. & Scotto di Santolo, A., 2005. Valutazione del ruolo degli strati pomicei nell'innesco dei fenomeni di colate di fango. Atti Conegno Nazionale "La mitigazione del rischio di colate di fango a Sarno e negli altri Comuni colpiti dagli eventi del maggio 1998", pp. 125-140.

Feddes, R. A., Kowalik, . P. J. .. & Zaradny, H., 1978. Simulation of field water use and crop yield. Monographs. Pudoc. Wageningen., p. 189.

Godt, J. et al., 2008. Transient deterministic shallow landslide modeling: Requirements for susceptibility and hazard assessments in a GIS framework. Engineering Geology, Vol. 102, pp. 214-226.

Guzzetti, F., Peruccacci, S., Rossi, M. & Stark, C. P., 2007. Rainfall thresholds for the initiation of landslides in central and southern Europe. Meteorology and Atmospheric Physics, Volume 98, Issue 3–4, p. 239–267.

Hungr O., Leroueil S., Picarelli L. (2014). The Varnes classification of landslide types, an update. Landslides, 11, pp.167–194.

Intrieri, E. et al., 2012. Design and implementation of a landslide early warning system. Engineering Geology, Volume 147-148, pp. 124-136.

Montgomery, D. R. & Dietrich , W. E., 1994. A physically based model for the topographi control on shallow landsliding. Water Resource Research, 30(4), pp. 1153-1171.

Mualem, Y., 1976. A new model for predicting the hydraulic conductivity of unsaturated porous media. Water Resources Research, 12(3), pp. 513-522.

Nicotera, M. V., Papa, R. & Urciuoli, G., 2010. An Experimental Technique for Determining the Hydraulic Properties of Unsaturated Pyroclastic Soils. Geotechnical Testing Journal, 33(5), pp. 1-22.

Nicotera, M. V., Papa, R. & Urciuoli, . G., 2015. The hydro-mechanical behaviour of unsaturated pyroclastic soils: An experimental investigation. Engineering Geology, Volume 195, pp. 70-84.

Papa, M. N., Medina, V., Ciervo, F. & Bateman, A., 2013. Derivation of critical rainfall thresholds for shallow landslides as a tool for debris flow early warning systems. Hydrol. Earth Syst. Sci., Volume 17, pp. 4095-4107.

Pirone, M., Papa, R., Nicotera, M. V. & Urciuoli, G., 2015. In situ monitoring of the groundwater field in an unsaturated pyroclastic slope for slope stability evaluation. Landslides, Volume 12, pp. 259-276.

Pirone, M., Papa, R., Nicotera, M. V. & Urciuoli, G., 2015. Soil water balance in an unsaturated pyroclastic slope for evaluation of soil hydraulic behaviour and bounday conditions. Journal of Hydrology, Volume 528, pp. 63-83.

Pirone, M., Papa, R., Nicotera, M. V. & Urciuoli, G., 2016. Hydraulic behaviour of unsaturated pyroclastic soil observed at different scales. Procedia Engineering, Volume 158, pp. 182-187.

Rigon, R. & Bertoldi, . G., 2005. GEOtop: A Distributed Hydrological Model with Coupled Water and Energy Budgets. JOURNAL OF HYDROMETEOROLOGY, Volume 7, pp. 371-388.

Santo A., di Crescenzo G., Forte G., Papa R., Pirone M., Urciuoli G. (2018). Flow-type landslides in pyroclastic soils on flysch bedrock in southern Italy: the Bosco de' Preti case study. Landslides, 15, pp. 63–82.

Savage, W. Z., Godt, J. W. & Baum, R. L., 2004. Modeling time-dependent areal slope stability. Landslides: Evaluation and Stabilization, pp. 27-36.

Shahabi , H. & Hashim, M., 2015. Landslide susceptibility mapping using GIS-based statistical models and Remote sensing data in tropical environment. Scientific Reports 5.

Sorbino, G. & Nicotera, M. V., 2013. Unsaturated soil mechanics in rainfall-induced flow landslides. Engineering Geology, Volume 165, pp. 105-132.

Wang, L.-J.et al., 2015. Landslide susceptibility mapping in Mizunami City, Japan: A comparison between logistic regression, bivariate statistical analysis and multivariate adaptive regression spline models. Catena, Vol.135, pp. 271-282.

LIST OF TABLES

TABLES

Table 1. Hydraulic Parameters for the soil A1 and C1

Soil	θ_s	θ_r	S_{res}	u_w^*	α	n	m	l	k_s
	-	-	-	kPa	1/kPa	-	-	-	m/s
A1	0.62	0.17	0	7	0.05	1.7	0.41	-1	$3.4\ 10^{-5}$
C1	0.67	0.198	0.065	7	0.015	1.7	0.41	-2.7	$1.7\ 10^{-6}$

Table 2. Hydraulic Parameters for the soil C2

θ_s	θ_r	α	n	m	λ	k_s
-	-	1/kPa	-	-	-	m/s
0.517	0.018	0.005	1.07	0.0654	0.273	$5\ 10^{-8}$

Table 3. Hydraulic parameters for the pumices in the low suction range.

$\vartheta_{sat,low}$	$\vartheta_{res,low}$	α_l	n_l	m_l
-	-	1/kPa	-	-
0.63	0.12	0.63	3	0.67

Table 4. Hydraulic parameters for the pumices in the high suction range.

$\vartheta_{sat,high}$	$\vartheta_{res,high}$	α_h	n_h	m_h
-	-	1/kPa	-	-
0.12	-0.12	0.02	2	0.5

Table 5. Mechanical properties for the soils.

SOIL	γ_{dry}	ϕ'	$n*$	Gs	c'
	kN/m^3	°	-	-	kPa
A1	8.06	37	0.69	2.65	5
C1	7.09	37	0.72	2.64	0
C2	10.64	37	0.57	2.49	0
P	4.8	40	0.8	2.55	0

Table 6. Geometric characteristics of the landslides under study.

LOCATION	Length	Depth	D/L
	m	m	
Gragnano	18	1.6	0.09
Corbara	24	2.3	0.096

TABLE OF FIGURES

Figure 20. Reduction function calibrated on the Gragnano soil profile.

Figure 21. Cancellation of the initial condition at the bedrock for a) Gragnano's model and b) Corbara's model.

Figure 22. Evolution of the Factor of safety profile from January 1996 to the 10th of January 1997 when the Landslide events occurred in Gragnano(a) and Corbara(b).

Figure 23 Evolution of the minimum Factor of safety profile from January 1996 to the 10th of January 1997 when the Landslide events occurred in Gragnano (a) and Corbara (b).

Figure 24. Pore water pressure profile at the time of the failure in Gragnano (a) and Corbara (b).

FIGURES

Figure 1. Main Somma-Vesuvio pyroclastic fall deposits (472 a.C; 79 a.C.; 3760 b.p. "Avellino eruption"; 8000 B.C."Mercato eruption") (Di Crescenzo & Santo, 2005)
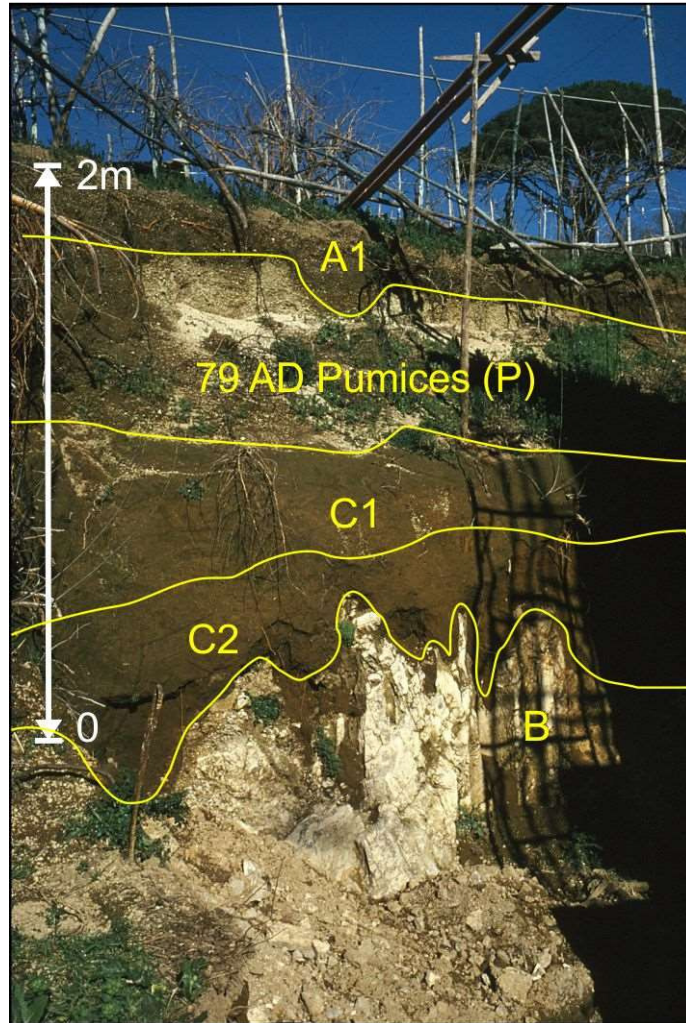
Figure 2. Outcrop of the stratigraphic sequence of the northern slope of Lattari Mts.
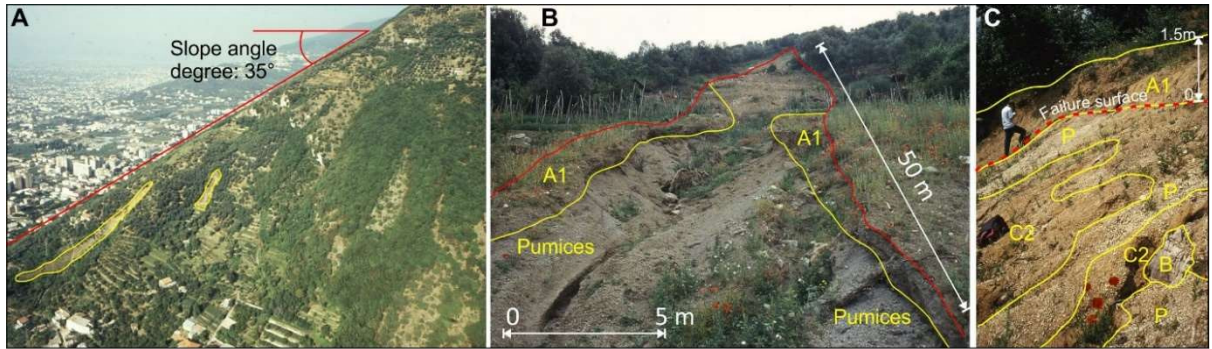
Figure 3. a) Structural slopes of Pendolo Mt. The yellow areas identify the two landslides occurred in 1997. b) Sub-triangular flow-like landslide Keys: A1= ash deposits. c) Transition zone of the Gragnano Landslide.
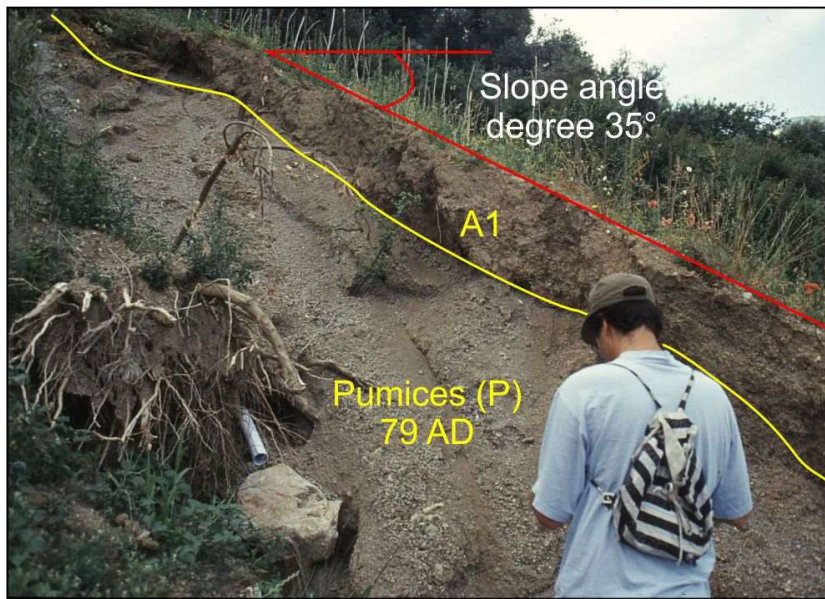
Figure 4. Transition zone of the Corbara.
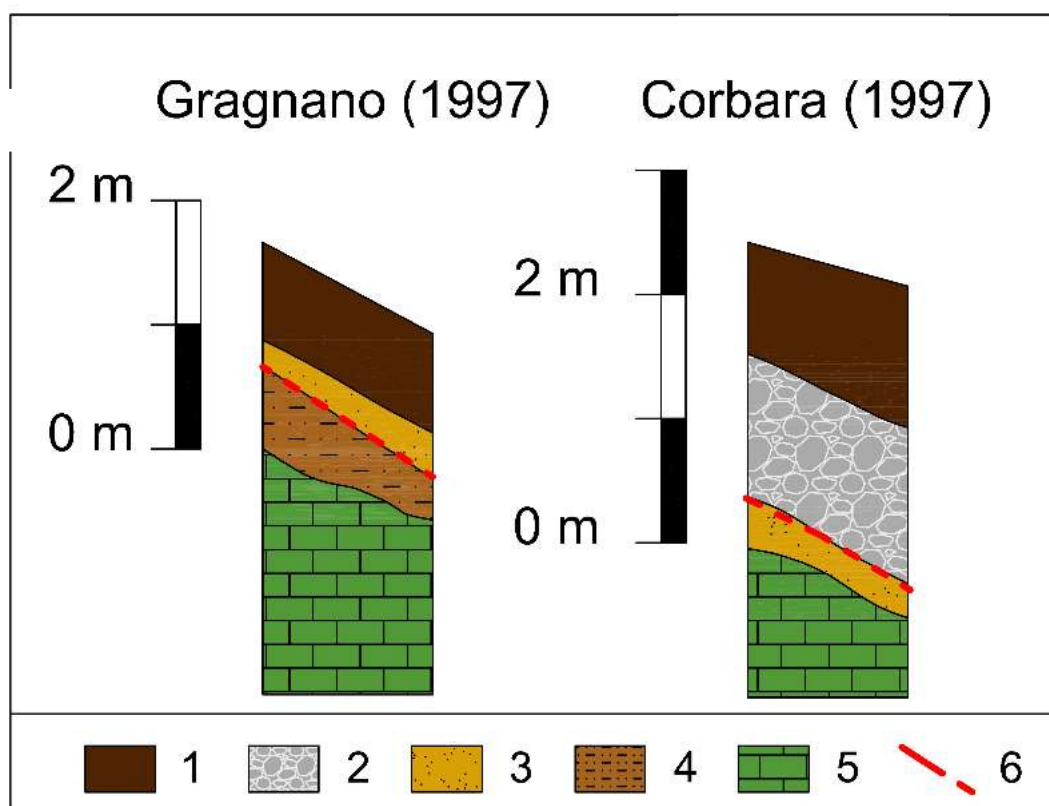
Figure 5. Soil profiles: 1) Pedogenized Pyroclastic Soil; 2) Pumices; 3) Ashes; 4) Compacted Ashes; 5) Bedrock; 6) Failure Surface.

1 & 2: Topsoil & ashy soil (0.00÷0.80 m)

3: Pumiceous deposits of
Avellino eruption (0.80÷1.50 m)

4: Palaeosoil (1.50÷2.30 m)

5: Pumiceous deposits of
Ottaviano eruption (2.30÷2.90 m)

6: Palaeosoil (2.90÷3.50 m)

7: Volcanic sand (3.50÷3.70 m)

8: Highly weathered fine-grained
ashy soil (3.70÷4.00 m)

Fractured limestone
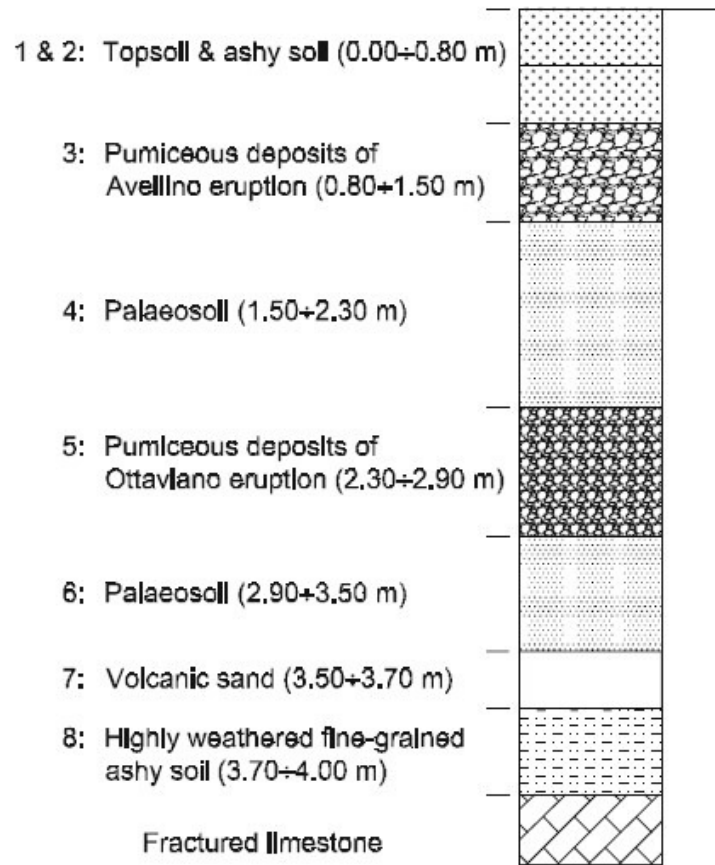
Figure 6. Typical soil profile in Monteforte Irpino (Pirone, et al., 2015)
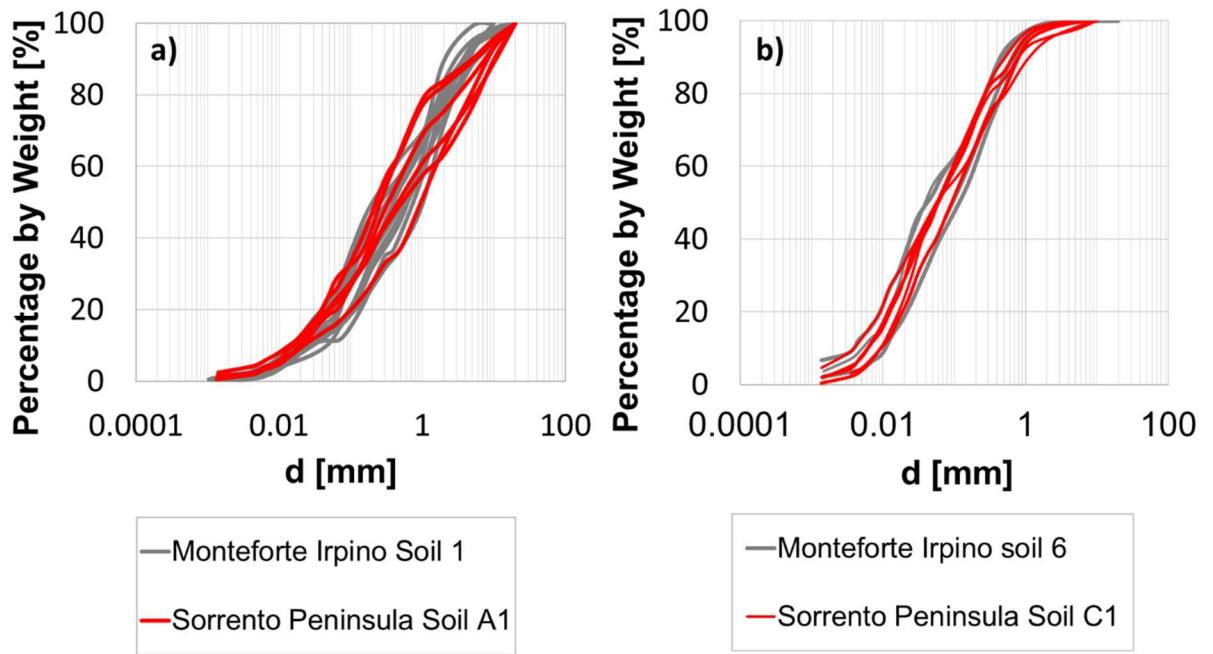
Figure 7. (a) Grain size distribution of soil 1 from Monteforte Irpino site and soil A1 of Sorrento Peninsula. (b) Grain size distribution of soil 6 from Monteforte Irpino site and soil C1 of Sorrento Peninsula.
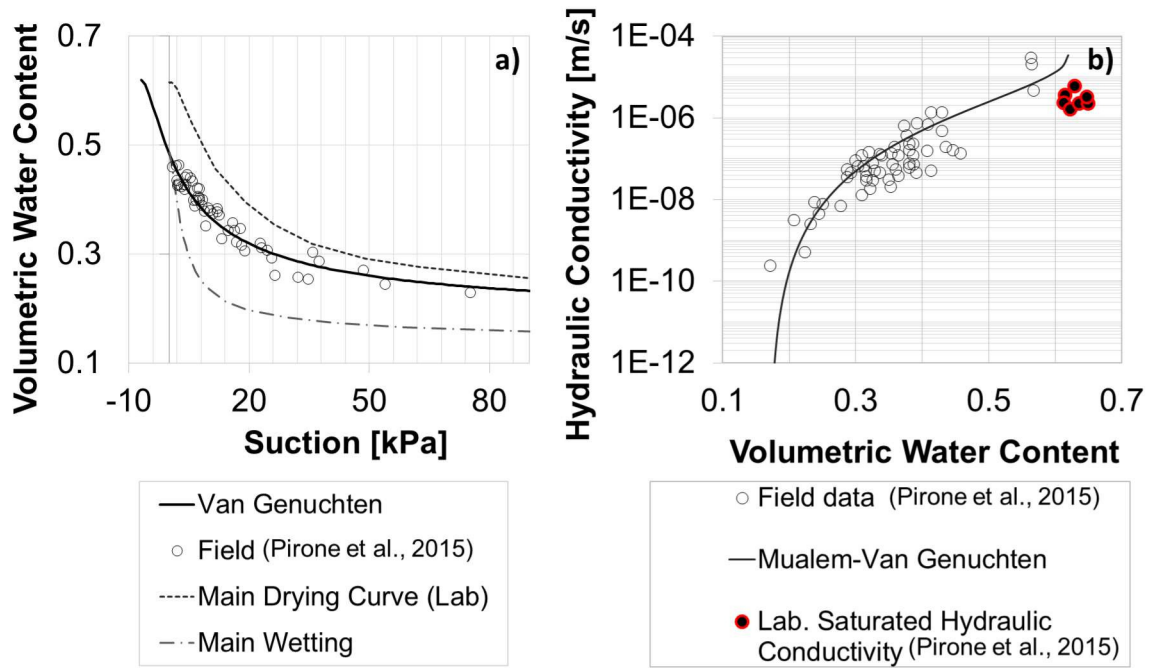
Figure 8. Water retention curve (a) and hydraulic conductivity (b) of the soil A1. (Pirone et al., 2015)
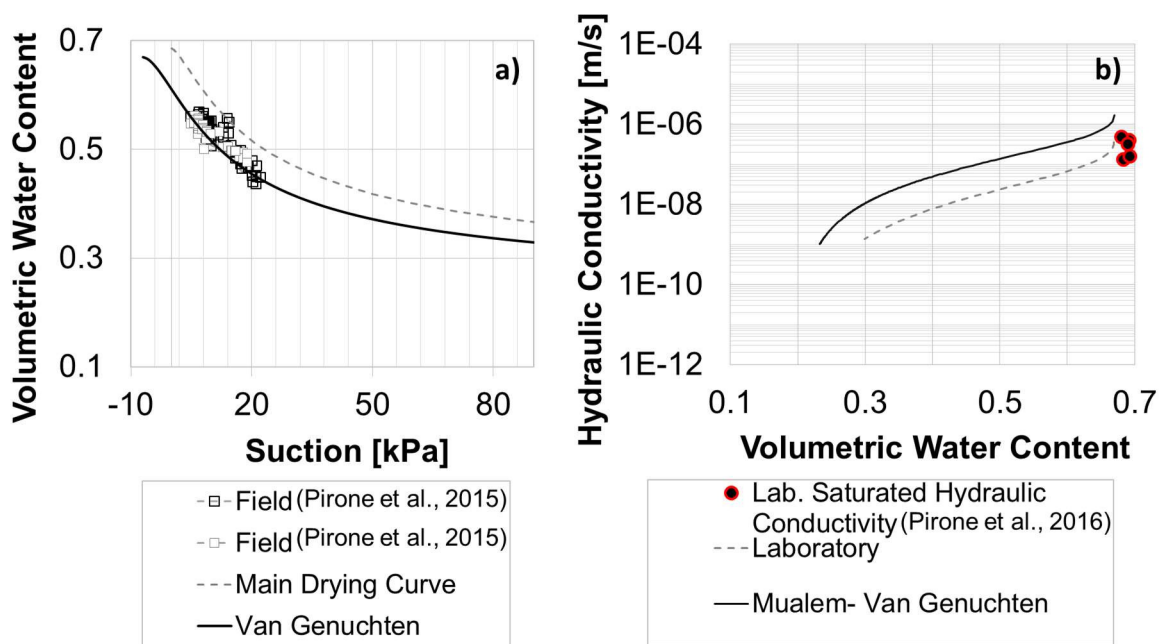
Figure 9. Water retention curve (a) and hydraulic conductivity (b) of the soil C1. (Pirone et al., 2015; Pirone et al., 2016)
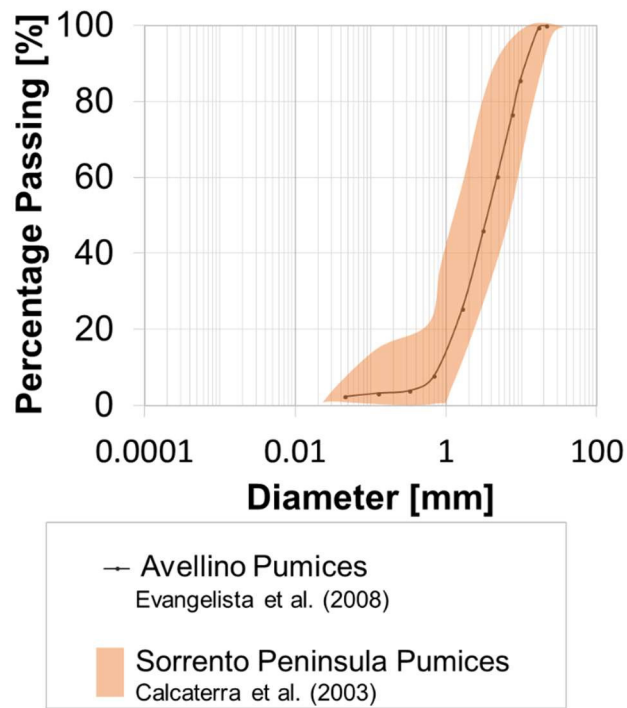
Figure 10. Comparison Grain size distribution of Sorrento Pumice (Calcaterra et al., 2003) and Avellino Pumice (Evangelista et al., 2008).
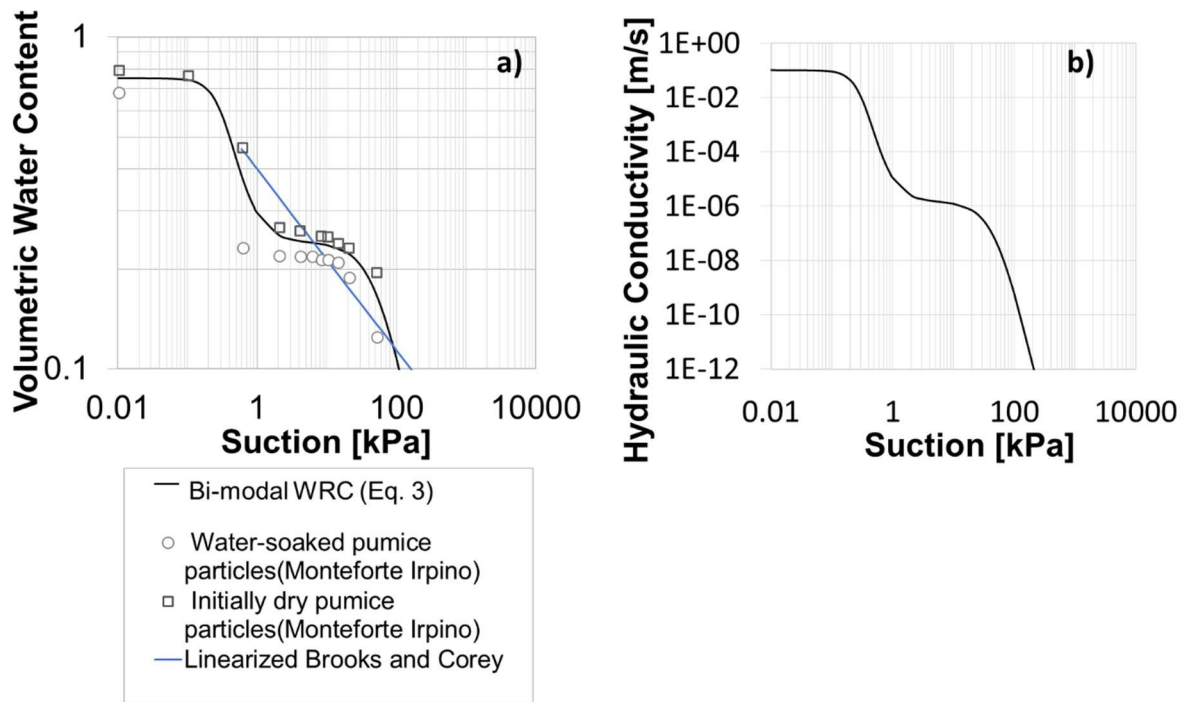
Figure 11. Water retention curve (a) and Hydraulic Conductivity Curve (b; Equation 4) for the pumices.
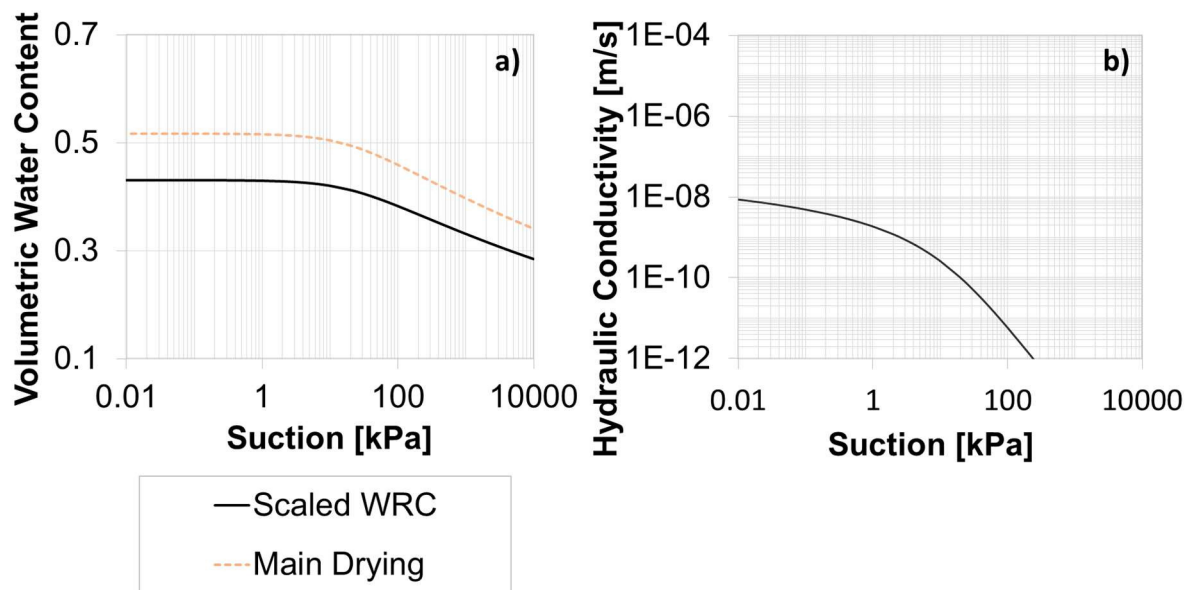
Figure 12. Water retention curve (a) and Hydraulic Conductivity (b) of the soil C2.
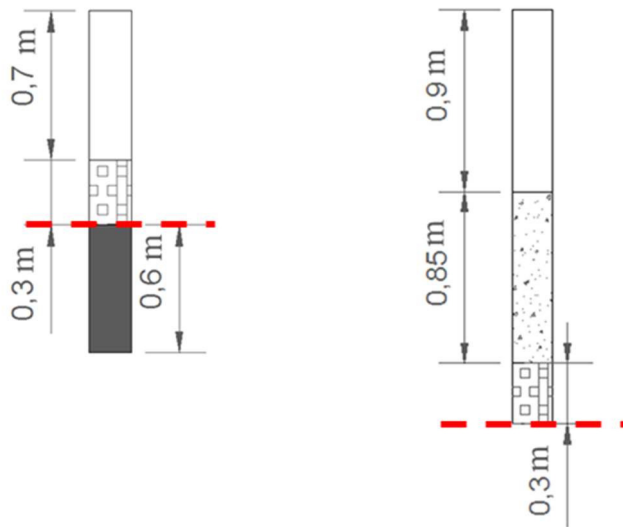
GRAGNANO   **CORBARA**

Pedogenized Pyroclastic Soil (A1)

Bedrock

Ashes (C1)

Compacted Ashes (C2)

Pumices (P)

- - - - Failure Surface

Figure 13. Soil profiles adopted in the analyses.
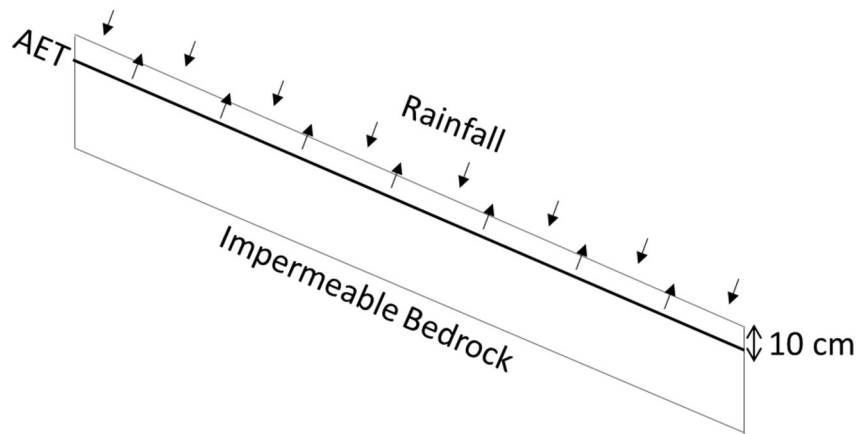
Figure 14. Scheme of the Boundary Conditions considered for the model.
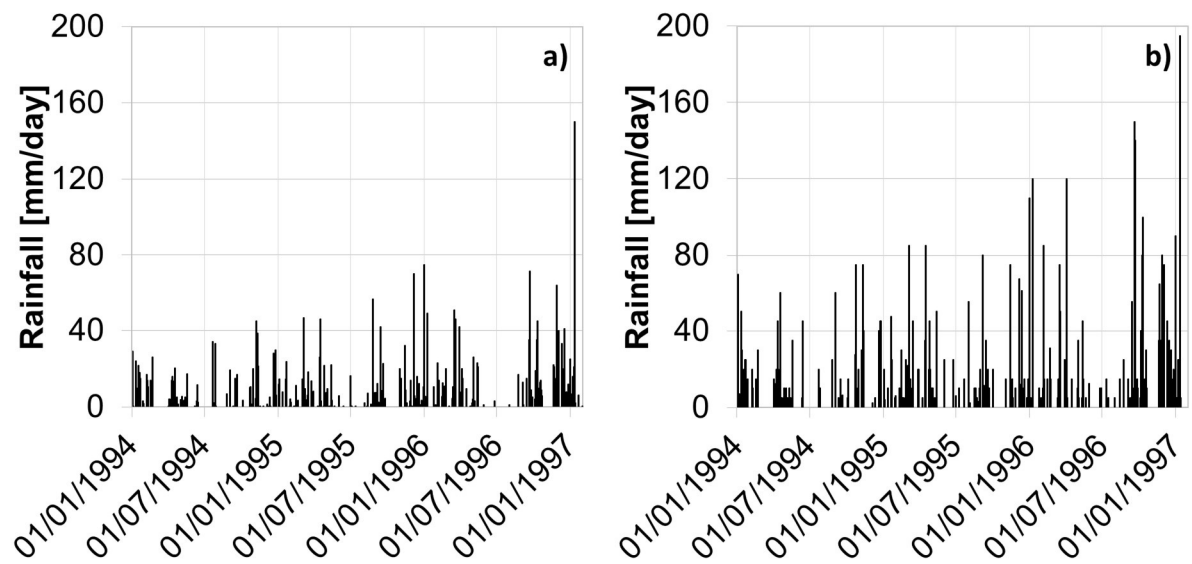
Figure 15. Rainfall from 1994 to 1997 registered by the pluviometer in Castellammare di Stabia (a) and Tramonti (b).
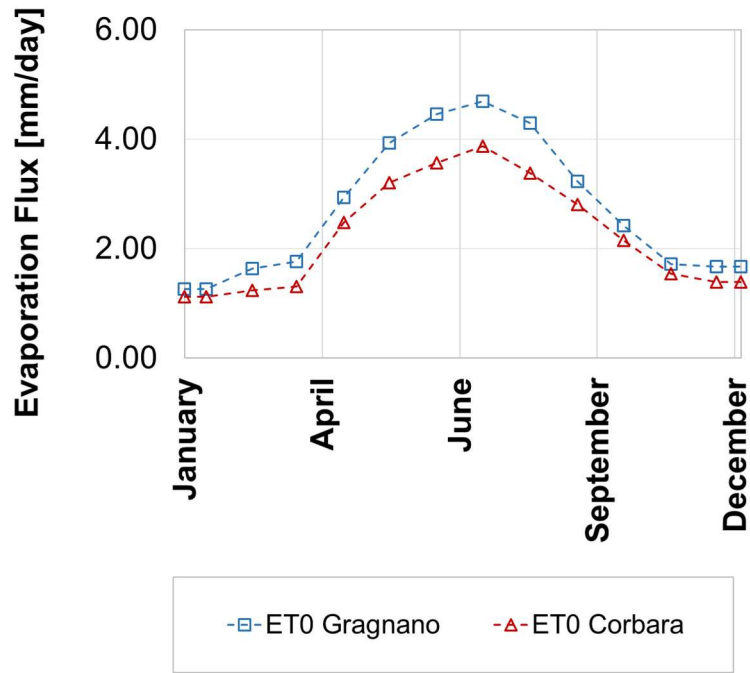
Figure 16. Monthly evaporation fluxes for Gragnano and Corbara.
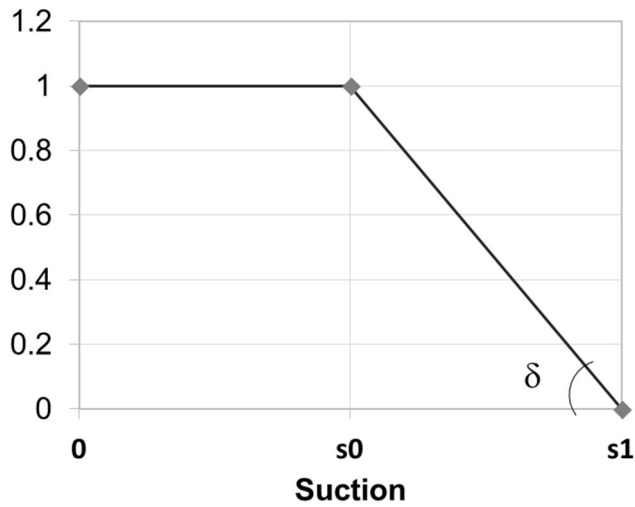
Error! Reference source not found.

Figure 17. Reduction function
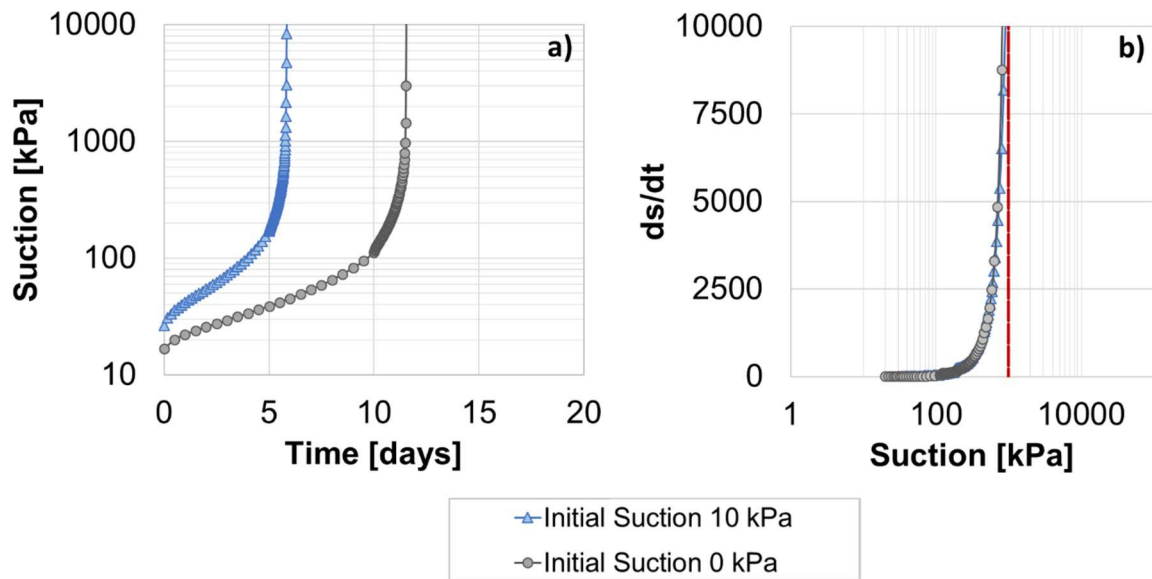
Figure 18. Identification of the limit suction value.
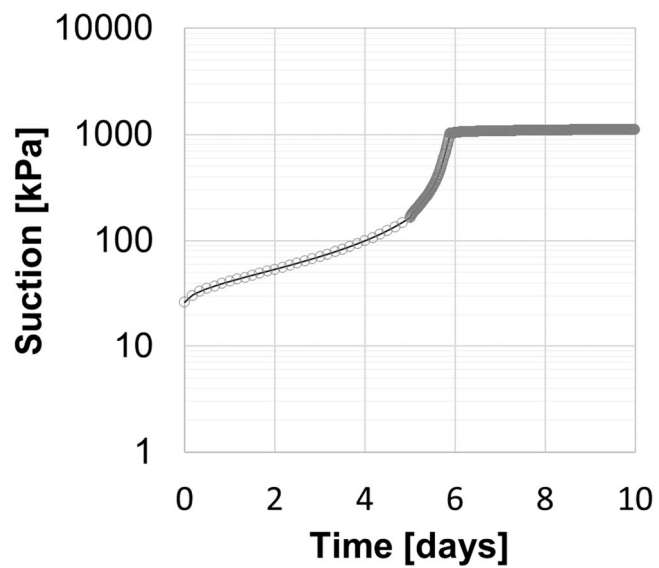
Figure 19. Identification of the value of suction at which the Actual Evapotranspiration goes to zero.

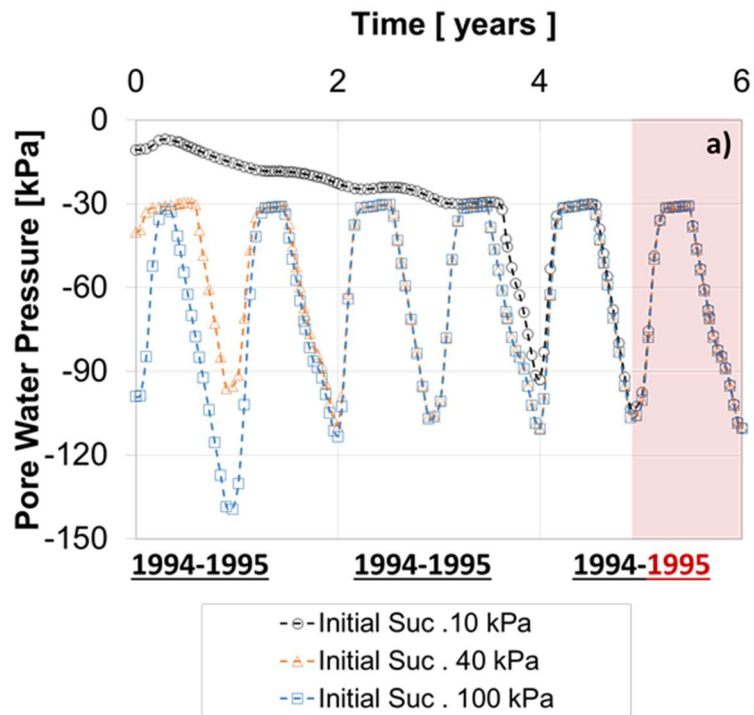**Figure 20. Reduction function calibrated on the Gragnano soil profile.**

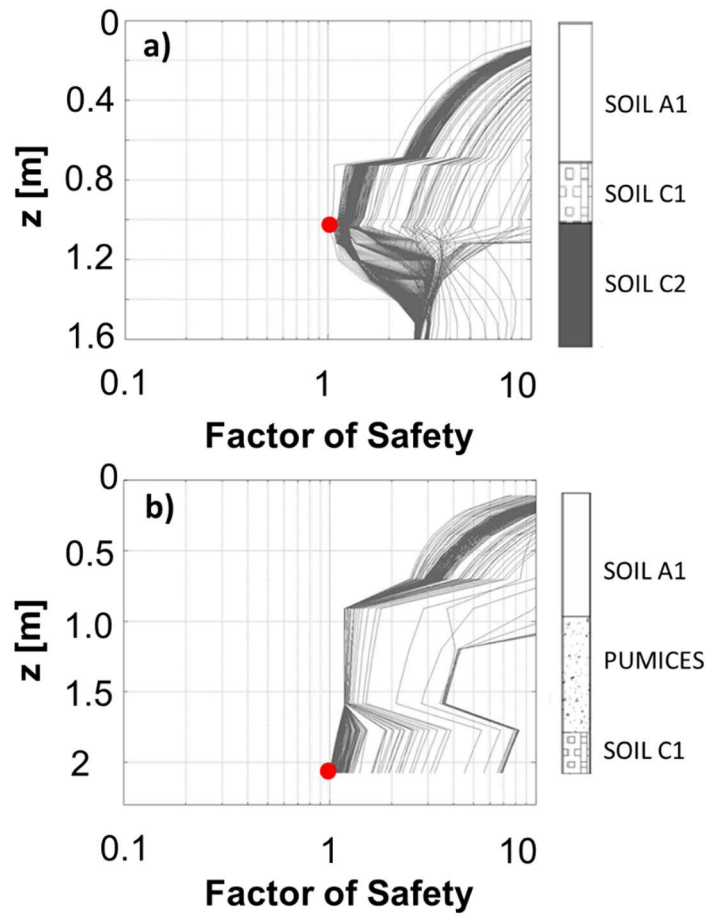**Figure 21.** Cancellation of the initial condition at the bedrock for a) Gragnano's model and b) Corbara's model.

Figure 22. Evolution of the Factor of safety profile from January 1996 to the 10th of January 1997 when the Landslide events occurred in Gragnano(a) and Corbara(b).
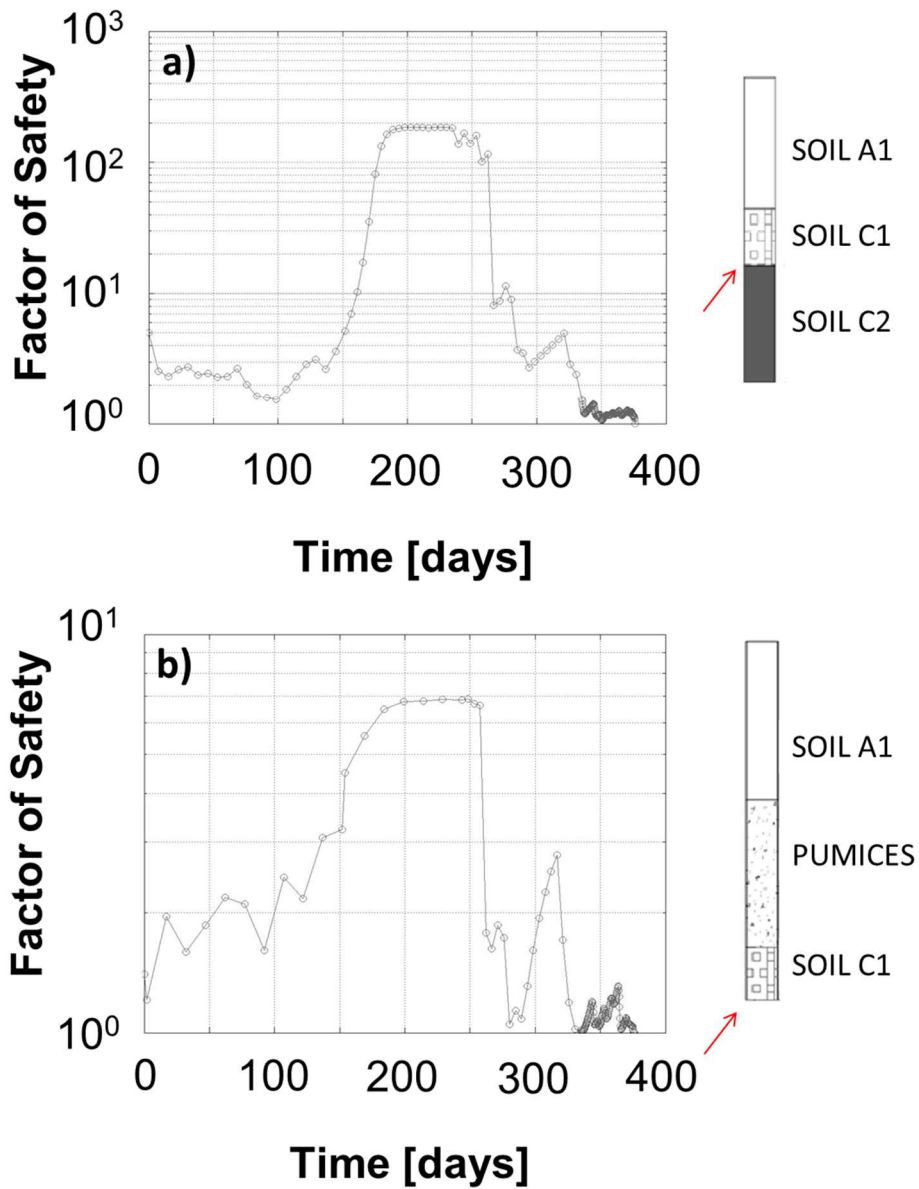
Figure 23 Evolution of the minimum Factor of safety profile from January 1996 to the 10th of January 1997 when the Landslide events occurred in Gragnano (a) and Corbara (b).
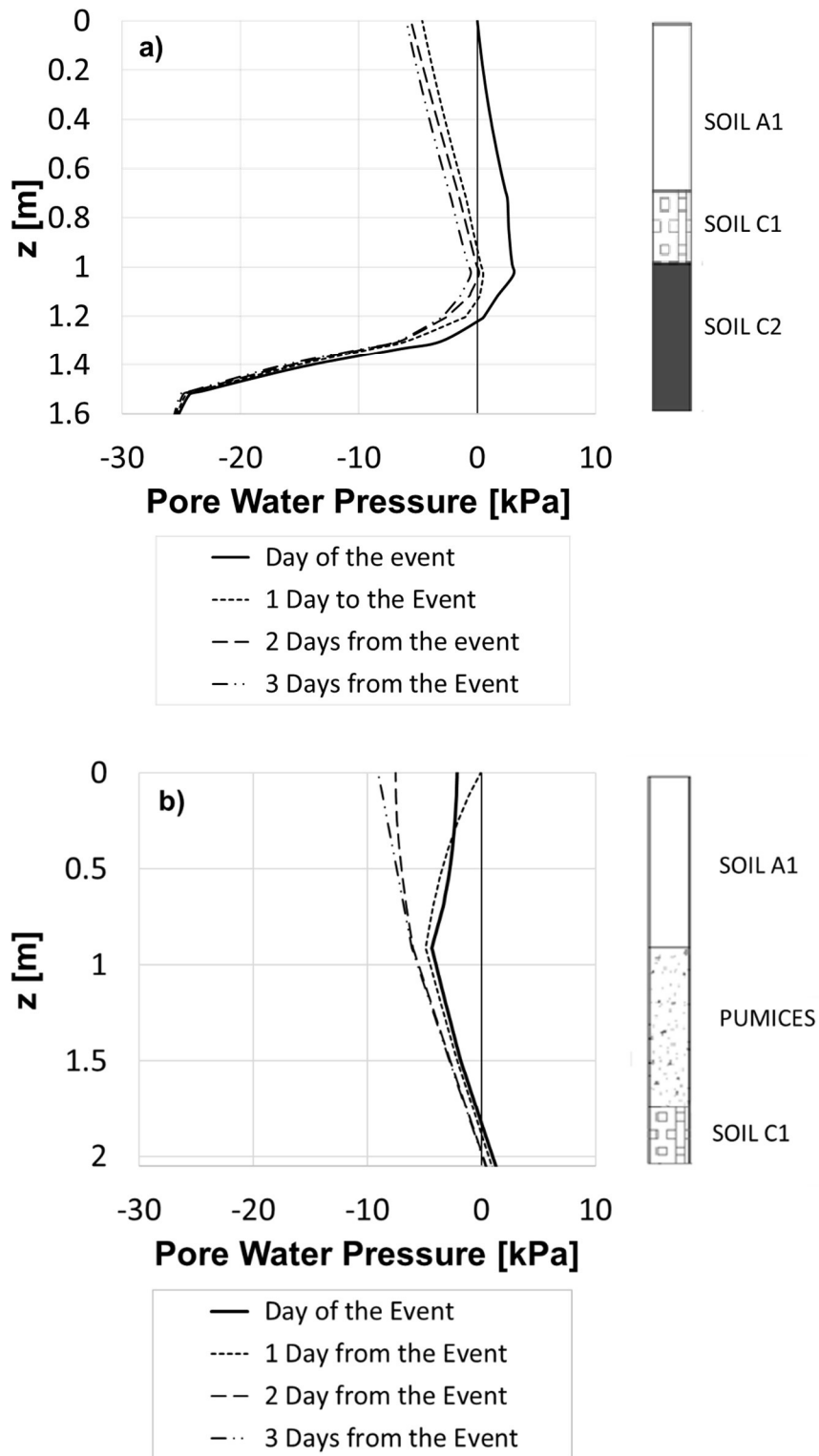
Figure 24. Pore water pressure profile at the time of the failure in Gragnano (a) and Corbara (b).